Phase decomposition

John Castagna[1], Arnold Oyem[2], Oleg Portniaguine[2], and Understanding Aikulola[3]

Abstract

Any seismic trace can be decomposed into a 2D function of amplitude versus time and phase. We call this process phase decomposition, and the amplitude variation with time for a specific seismic phase is referred to as a phase component. For seismically thin layers, phase components are particularly useful in simplifying seismic interpretation. Subtle lateral impedance variations occurring within thin layers can be greatly amplified in their seismic expression when specific phase components are isolated. For example, the phase component corresponding to the phase of the seismic wavelet could indicate isolated interfaces or any other time symmetrical variation of reflection coefficients. Assuming a zero-phase wavelet, flat spots and unresolved water contacts may show directly on the zero-phase component. Similarly, thin beds and impedance ramps will show up on components that are 90° out of phase with the wavelet. In the case of bright spots caused by hydrocarbons in thin reservoirs because these occur when the reservoir is of an anomalously low impedance, it is safe to assume that the brightening caused by hydrocarbons occurs on the component −90° out of phase with the wavelet. Amplitudes of other phase components associated with bright reflection events, resulting perhaps from differing impedances above and below the reservoir, thus obscure the hydrocarbon signal. Assuming a zero-phase wavelet, bright-spot interpretation is thus greatly simplified on the −90° phase component. Amplitude maps for the Teal South Field reveal that the lateral distribution of amplitudes is greatly different for the original seismic data and the −90° phase component, exhibiting very different prospectivity and apparent areal distribution of reservoirs. As the impedance changes laterally, the interference pattern for composite seismic events also changes. Thus, waveform peaks, troughs, and zero crossings, may not be reliable indicators of formation top locations. As the waveform phase changes laterally due to lateral rock properties variations, the position of a formation top on the waveform also changes. By picking horizons on distinct phase components, this ambiguity is reduced, and more consistent horizon picking is enabled.

Introduction

Spectral decomposition (Partyka et al., 1999) maps a 1D seismic trace of amplitude versus time $S(t)$ into 2D functions of time-localized amplitude spectra versus time $A(f,t)$ and phase spectra versus time $\theta(f,t)$. There is a wealth of information contained in the instantaneous phase spectra at any given time that is often difficult to interpret. For example, Figure 1 shows a time-frequency analysis for amplitude and phase using different spectral decomposition methods. Although the methods differ in their temporal and frequency resolutions, the amplitude-frequency-time mappings are somewhat similar and straightforward to understand. The phase spectra, however, are very complicated and differ greatly between the methods. As a consequence, conventional phase-frequency-time spectra are rarely directly used for seismic interpretation purposes.

Another approach to understanding the phase of a seismic trace is to distribute the amplitude and phase spectra so that the amplitude can be expressed as a function of phase as well as frequency. Here, we require that the spectral decomposition method used produces a time-frequency analysis that sums to the seismic trace (conserves energy) when integrated over frequency (for example, using the continuous wavelet transform [CWT]; e.g., Chakraborty and Okaya [1995], or constrained least-squares spectral analysis [CLSSA]; Puryear et al., 2012). Then,

$$S(t) = \int S'(f,t)df, \tag{1}$$

where $S'(f,t)$ is the time-frequency analysis, and the integration is over all frequencies. Note that at any time t, the instantaneous spectrum $S'(f)$ is not a Fourier transform of the trace, and recovery of the original trace from the time-frequency analysis is a simple summation over frequency rather than an inverse Fourier transform. This

[1]University of Houston, Department of Earth and Atmospheric Sciences, Houston, Texas, USA. E-mail: jpcastagna@uh.edu.
[2]Lumina Technologies Inc., Research and Development, Houston, Texas, USA. E-mail: arnold.oyem@luminageo.com; oleg.portniaguine@luminageo.com.
[3]Shell Exploration & Production Company, Upstream America Deepwater, Houston, Texas, USA. E-mail: niyiaikulola@yahoo.com.

Manuscript received by the Editor 4 September 2015; revised manuscript received 24 November 2015; published online 18 July 2016; corrected version published online 16 August 2016. This paper appears in *Interpretation*, Vol. 4, No. 3 (May 2016); p. SN1–SN10, 10 FIGS.
http://dx.doi.org/10.1190/INT-2015-0150.1.

is achievable because the process of mapping a 1D function of time into a 2D function of time and frequency is inherently nonunique, and a particular time-frequency analysis can be constrained to obey equation 1. This results in conservation of energy across frequency. Further, it is also possible to require that

$$S'(f,\theta,t) = A(f,t)\cos\theta(f,t), \tag{2}$$

where we have now introduced phase as a third dimension. The amplitude and phase spectra can thus be collapsed into a simple 2D function by

$$S'(\theta,t) = \int_{f_1}^{f_2} S'(f,\theta,t)df, \tag{3}$$

where f_1 and f_2 define the frequency band of interest. We refer to the function $S'(\theta,t)$ as a phase gather that shows the distribution of seismic amplitude versus phase as a function of time. The phase gather is intuitively interpretable as representing the amplitude versus time of individual phase components of the seismic trace. We have

$$S'(t) = \int_{\theta_1}^{\theta_2} S'(\theta,t)d\theta, \tag{4}$$

where θ_1 and θ_2 represent a phase band of interest. Figure 2 shows a phase gather derived from a seismic trace using CLSSA and passing all frequencies. The CLSSA is preferred over the CWT for this process because it retains the resolution of the data rather than smoothing over time as the CWT does at low frequencies (Puryear et al., 2012). When all phases and frequencies are included using wide-open passbands of frequency and

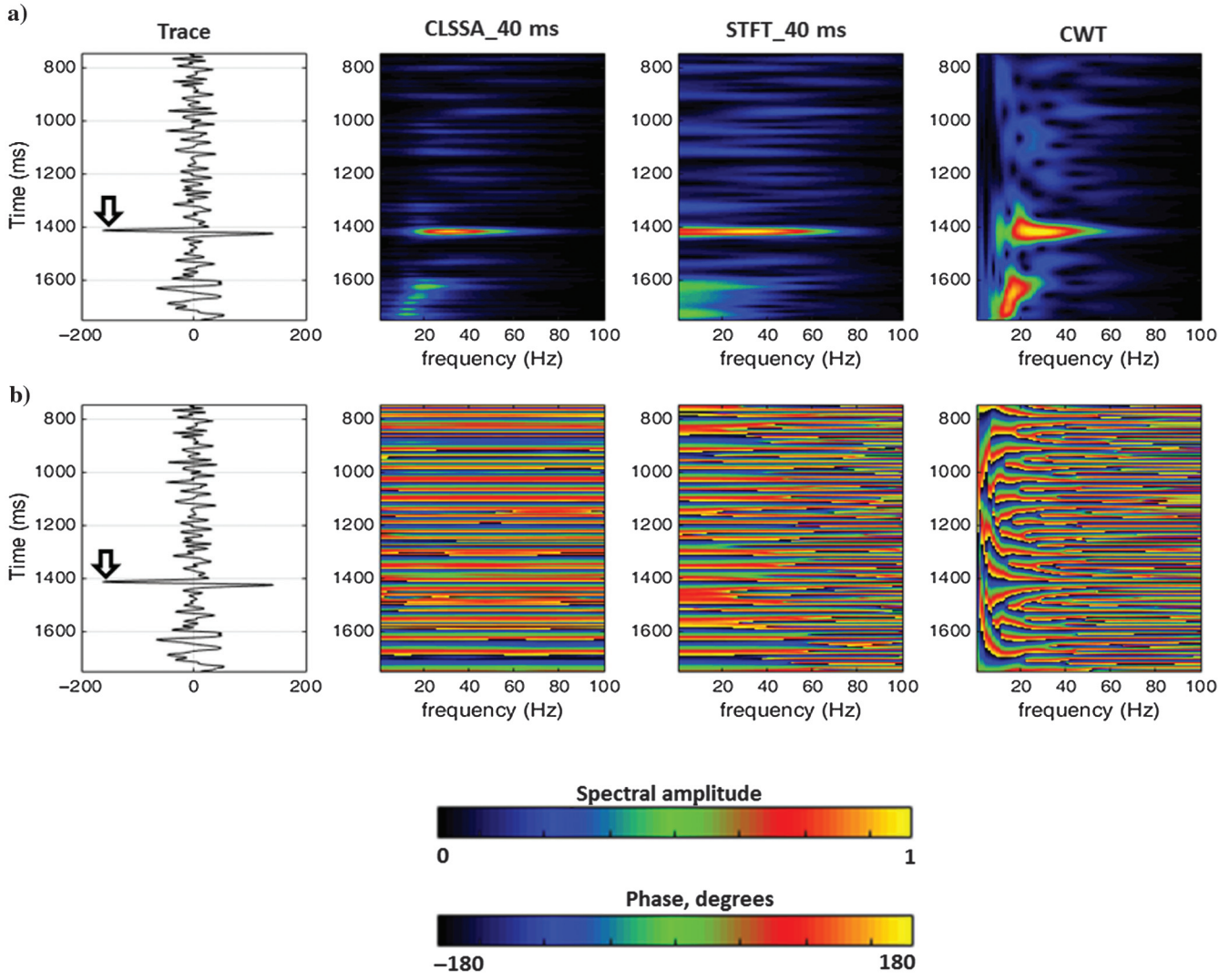

Figure 1. Amplitude magnitude and phase time-frequency analyses of a real seismic trace generated from several spectral decomposition techniques. CLSSA is a constrained least-squares spectral analysis (Puryear et al., 2012) using a 40 ms sliding time window. STFT is the short-time Fourier transform with a 40 ms window. CWT is the continuous wavelet transform with a Morlet wavelet dictionary. (a) amplitude spectra and (b) phase spectra. The white arrow points to a hydrocarbon reservoir bright spot.

phase, then $S'(t) = S(t)$, and the original seismic trace is reconstructed by equation 4.

Equation 3 is an example of phase decomposition of the seismic trace. The complete operation defined by equations 1–4) represents a type of phase filtering of the seismic trace, in which only desired phase components within specified frequency bands are included in the phase-filtered output $S'(t)$. Phase filtering is a potentially powerful interpretation tool in that it can be used to suppress or accentuate seismic events with specified spectral characteristics. Alternatively, if no filtering is desired, one can uniquely decompose the phase by separating real and imaginary components of the time-localized spectrum (in either the time or frequency domain) and reconstructing any response phase by combinations of these.

Synthetic examples

Phase decomposition is particularly useful in the case of seismically thin layers, in which interference between reflections from the top and base of a layer causes the phase of the response to differ from the wavelet phase. Interpretation of phase-decomposed data is most straightforward when the wavelet can be assumed to be zero phase. For simplicity, the examples in this paper use or assume zero-phase wavelets. In practice, the method can be applied to data of any phase, providing the results are interpreted accordingly. As our synthetic examples are meant to be only illustrative, we use Ricker wavelets in all cases because these are readily interpretable.

The first synthetic example (Figure 3) is that of an intermediate impedance thin layer (the layer time thickness equals one-quarter of the dominant wavelet period) between half-spaces of lower impedance above and higher impedance below. Within that layer, there is a channel with reduced impedance relative to the interchannel facies. The synthetic seismogram (Figure 3b) shows a "hard" (positive) reflection resulting from the overall impedance increase. The synthetic response is almost zero phase because the reflection coefficients at the top and base of the layer are almost equal. The amplitude variation caused by the channel is small enough that it would not be readily recognized on the conventional seismic data. The lateral impedance change, caused by the channel, has the effect of making the positive reflection coefficient at the top of the layer slightly smaller and the reflection coefficient at the base of the layer slightly larger. Because this is a thin bed, the effect on the overall amplitude and phase is visually small, as evidenced by inspection of the synthetic waveforms. So any amplitude anomaly or phase anomaly caused by the channel would be weak at best when calculated directly on the seismic trace. On the other hand, the −90° phase component of the data shows a strong obvious amplitude anomaly (Figure 3c). It literally transforms a previously

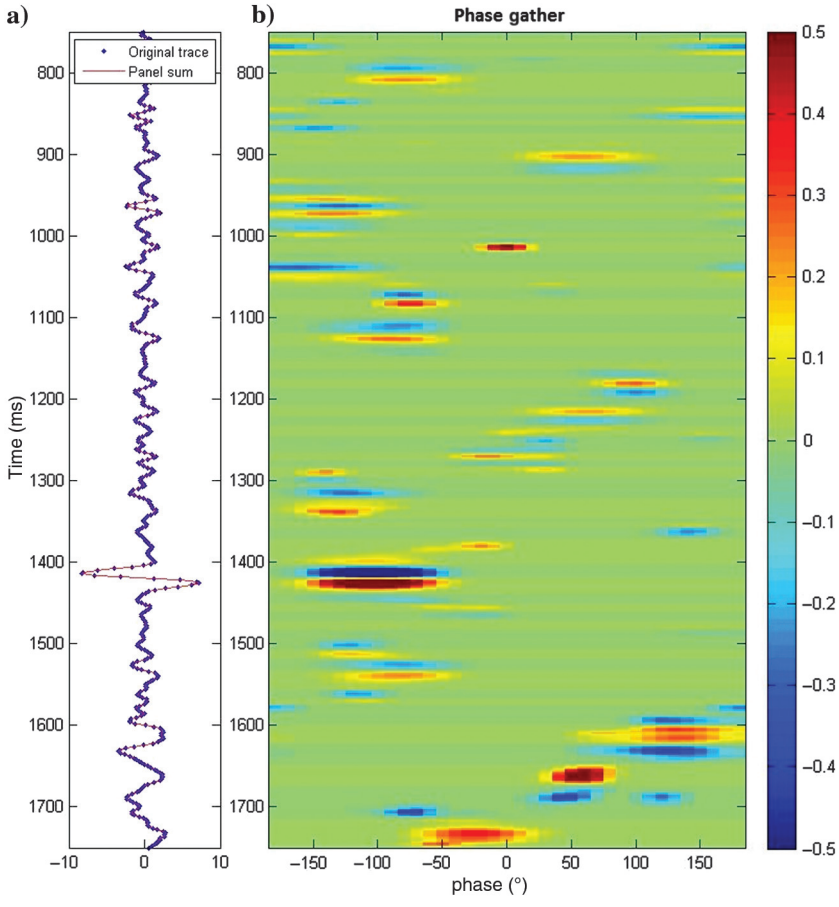

Figure 2. Phase decomposition. (a) seismic trace (blue points) and summed phase gather (red line), obtained by summing the time-phase panel over phase to reconstruct the seismic trace and (b) phase gather. Unlike a phase spectrum or attribute, the phase gather shows the amplitude and phase information simultaneously.

almost invisible channel into a highly anomalous one. Figure 4 is a more detailed look at this phenomenon on a single trace. The thin, intermediate impedance layer has almost equal reflection coefficients at its top and base. With a low-frequency wavelet, this symmetrical pair acts almost as a single reflection coefficient with the summed magnitudes of the pair. The result is that the zero-phase component of the data is almost identical to the synthetic waveform, whereas the sum of the ±90° components is small. (The sum of the ±90° components is a useful attribute to use when one does not know the direction of the impedance variation.) A slight impedance change in the intermediate layer corresponding to an approximately 10% change in the reflection coefficients causes the top reflection coefficient to become more negative and the bottom one to become more positive (Figure 4b). With a low-frequency seismic wavelet, this pair has almost the same summed magnitude as the symmetrical case, so there is little change in the seismic amplitude and the zero-phase component is still very similar to the synthetic trace. On the other hand, the slight asymmetry in reflection coefficients resulting from the seismic trace shows up strongly on the ±90° component sum.

In many cases, for thin layers, the change in waveform caused by an anomalously low impedance appears on the −90° component, and conversely, the change in waveform caused by an anomalously high impedance occurs on the +90° component. Such anomalies are most obvious when the layer is inter-

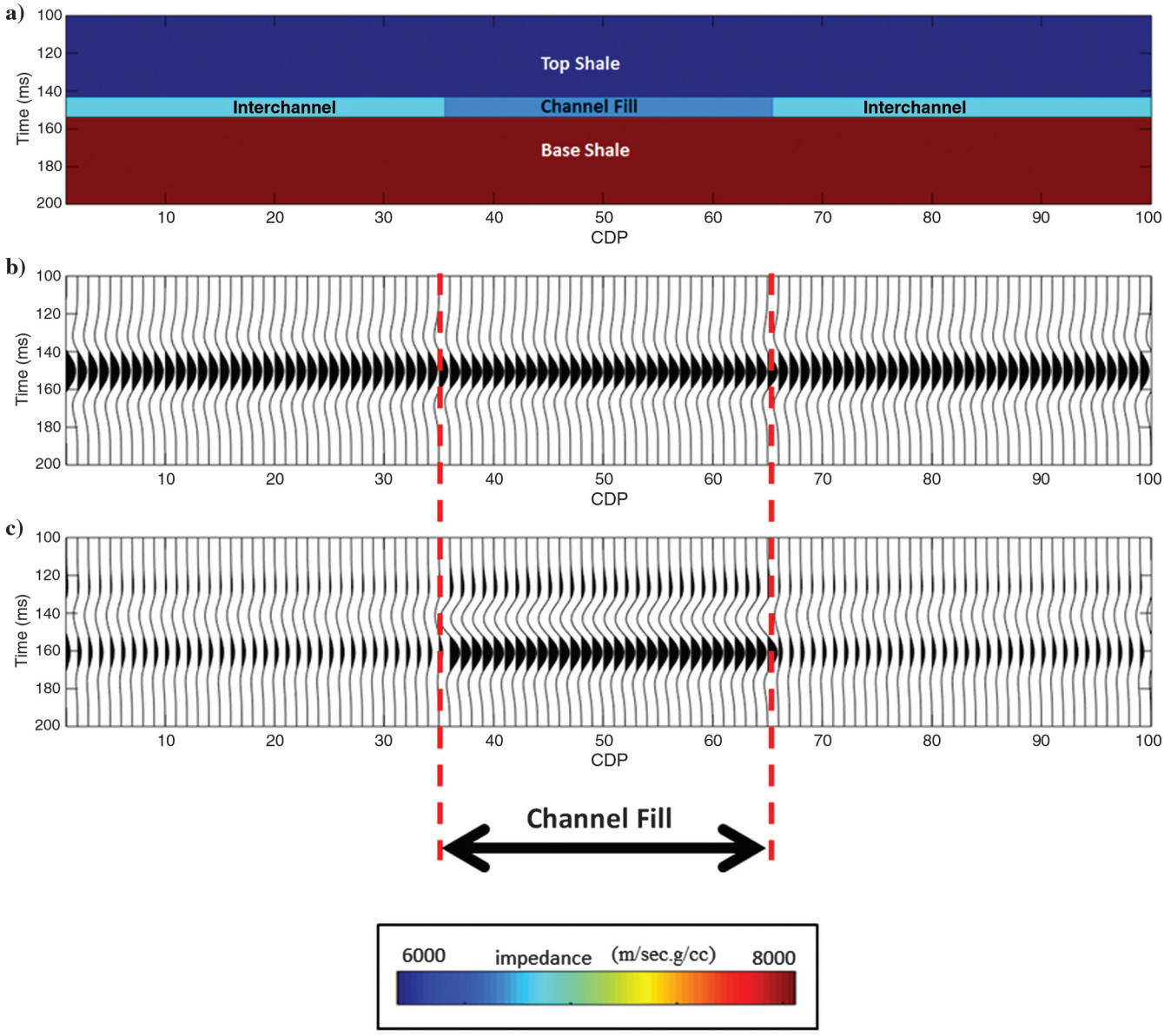

Figure 3. (a) Impedance model, (b) synthetic seismic, (c) −90° phase component. The amplitude anomaly due to the change in impedance in the thin layer containing the channel, though not very apparent on the synthetic seismogram, causes a strong amplitude anomaly on the −90° phase component.

mediate in impedance, but in many cases, the lateral impedance changes in a seismically thin layer of any impedance relative to the surrounding layers are most visible on the ±90° components. This discussion suggests that phase decomposition can potentially aid in the direct interpretation of the data in terms of impedance variations.

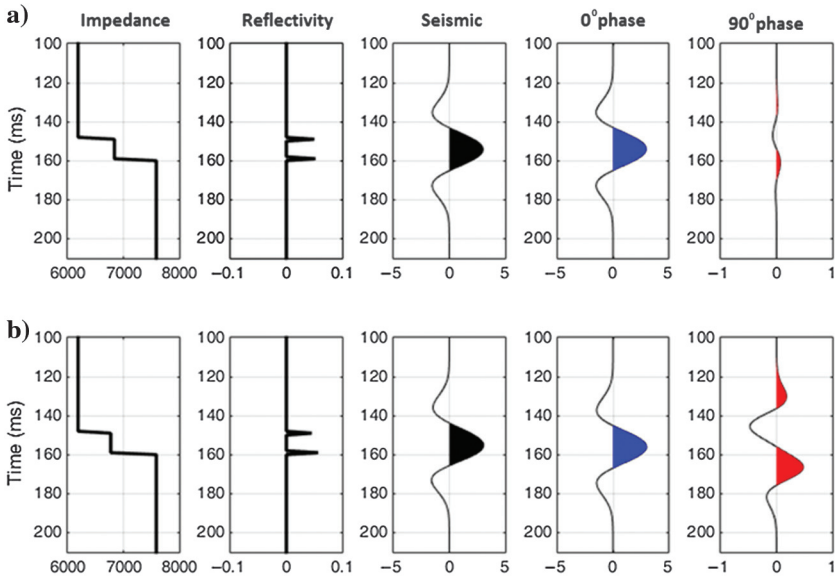

Figure 4. (a) Initial model. The reflection coefficients are almost equal, so the zero-phase component dominates (b) perturbed model. The ±90° component shows a large amplitude anomaly not readily evident on the original seismic trace or on the zero-phase component.

To the extent that the convolutional model is valid and with the caveats above, we can conclude that isolated interfaces will appear best on the component that corresponds to the phase of the wavelet, and thin layers with reflection coefficients of opposite sign at top and base will be strongest on a ±90° component. We also know that long impedance ramps can produce ±90° responses, and thin layers of alternating high and low impedance, as might be caused by a water contact in a thin layer, can produce a zero-phase response. More complex stratigraphic variations can produce diagnostic mixed-phase responses. Thus, phase decomposition can be of great interpretive value.

The use of phase decomposition for thin bed detection is illustrated in Figure 5, which shows a conventional wedge model synthetic (following the example of Widess, 1973). As seen in Figure 5a, the wedge is thicker (well above tuning) to the right and the reflections from the top and base exhibit the phase of the wavelet (zero phase in this case). To the left, the layer thins and the top and base reflections interfere. In the vicinity of tuning and below, the waveform response phase is approximately −90°. In such a situation, phase decomposition readily separates the thin (Figure 5b) and thick (Figure 5c) parts of the wedge.

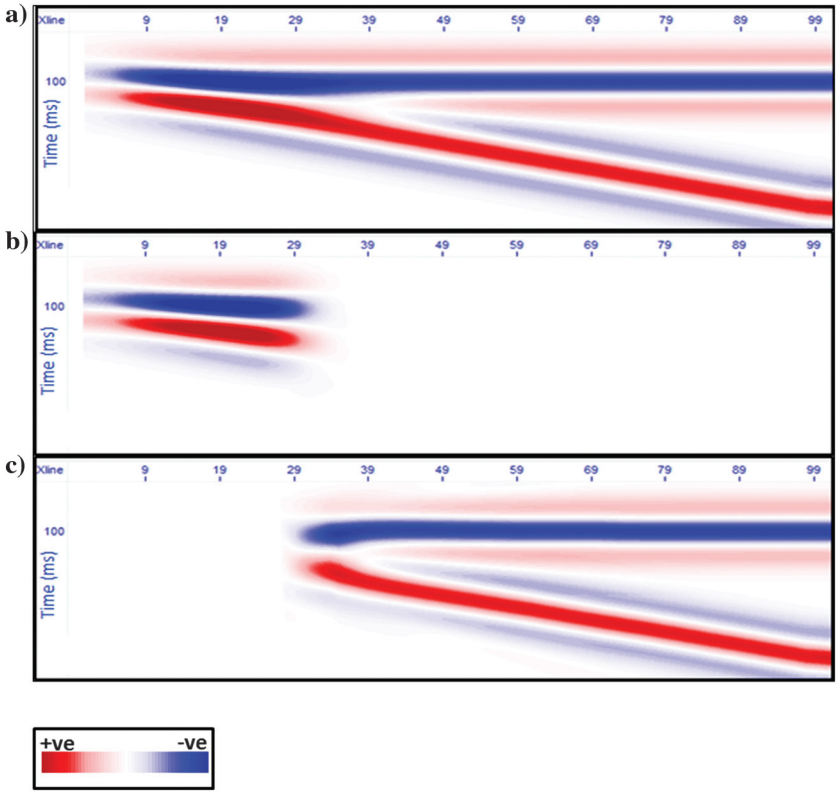

Figure 5. (a) Wedge model, (b) −90° phase component, and (c) 0° phase component.

In a thin layer, it can be difficult to directly observe hydrocarbon-water-contact reflections that may go unrecognized. Figure 6 shows the case of a thin layer in which the introduction of gas flips the reflection polarity from peak over trough for brine-filled rock and to trough over peak for gas-filled rock. Because the layer is thin, the water contact cannot be resolved and an interference pattern results. The summed ±90° components (Figure 6c) show the gas and brine legs, relatively undisturbed by the water-contact reflector, whereas the zero-phase component (Figure 6d) shows the water-contact contribution, which can be seen to have positive polarity, as water contacts generally should. Note that the contact reflector is not flat as a true flat spot should be. This is because this is not an isolated reflection from a single reflector, but rather it is the response from two thin layers of alternating impedance. At the spatial position where the gas sand and brine intervals have the same time thickness, the reflectivity series is essentially a second-derivative operator, which is zero phase. At other positions, this is no longer strictly true, so the apparent arrival time changes. In this case, the correct arrival time for the flat spot can be found at the spatial position of the polarity reversal seen on the ±90° components (Figure 6b).

Real data examples

The Teal South Field (Pennington et al., 2001) is on the offshore Gulf of Mexico shelf in the Eugene Island area. The region is characterized by bright spots associated with seismically thin reservoirs. These typically show a very distinctive bright trough/peak response on conventional seismic data and make for relatively easy bright-spot interpretation. However, even in this apparently simple interpretation situation, there can be ambiguities. For example, Figure 7a shows a seismic section across the field that exhibits obvious amplitude anomalies. However, not all of the bright events have the distinctive trough/peak response, and the magnitude of the anomalies is variable depending on the layer thickness. Interference with other reflections sometimes obscures the bright-spot interpretation. By plotting only the −90° component (Figure 7b), most of the interfering reflections are reduced, the amplitudes are

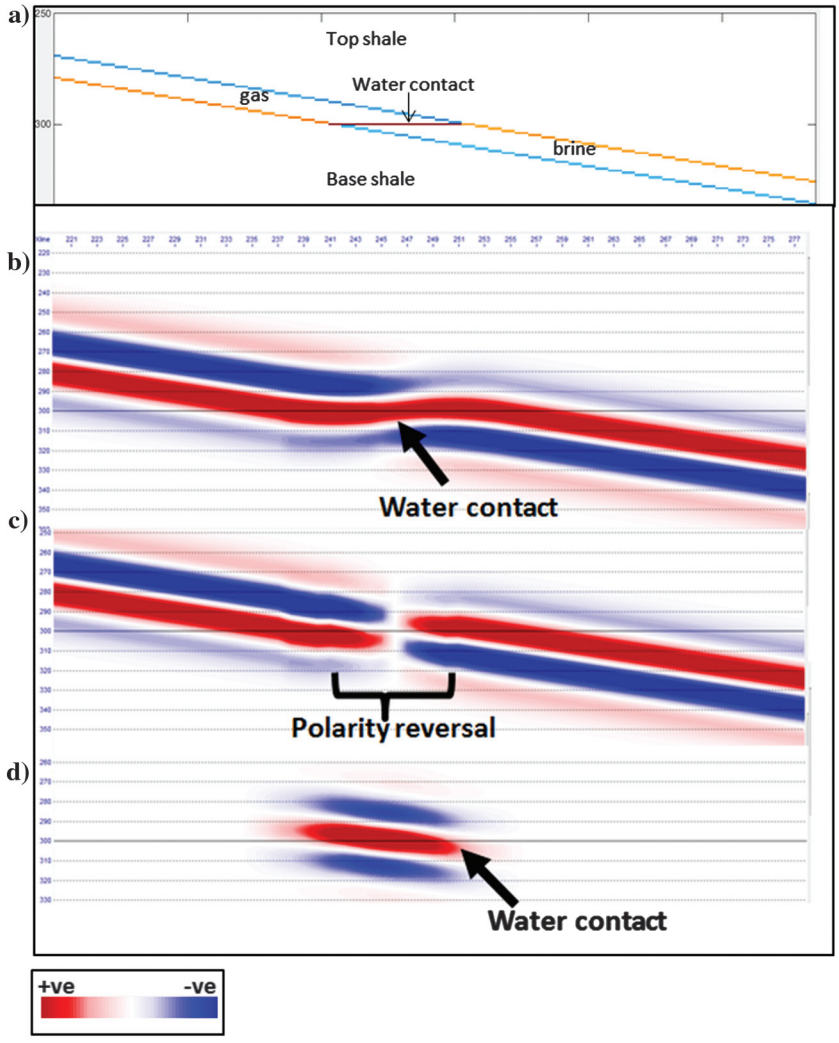

Figure 6. (a) Geologic model showing a thin reservoir with a water contact, (b) synthetic seismic section, (c) summed ±90° phase components, and (d) 0° phase component.

more uniformly anomalous, and only events with the desired trough/peak response appear. The result is a greatly simplified, and very different, amplitude interpretation for seeing thin beds below tuning. The value of phase decomposition becomes most evident in map view. Figure 8a is the maximum magnitude map, within a constant seismic window (Figure 8b). A known productive interval is marked with an R to the lower right and a possibly prospective bright event is marked with a B. On the −90° component (Figure 9), the reservoir remains bright, but amplitude B disappears. Also, along the dashed line of the displayed seismic section, previously unremarkable amplitudes on the original seismic are highly anomalous on the −90° component. It is important to understand that bringing out anomalies by observing them on distinct phase components is not equivalent to weighting the amplitudes by a function of the instantaneous phase, and it certainly is not equivalent to a phase rotation. What is being seen is that fraction of the amplitude exhibiting the specified phase characteristics (−90° in this case) with extraneous superposed interfering amplitudes exhibiting other phase behavior is removed. Amplitude maps for specific phase components can be very different from conventional amplitude maps, showing different prospectivity and different areal extent of prospects.

Figure 10 shows the impact of phase separation on a process as fundamental as horizon picking on a real data set showing a sequence of "railroad-track" reflections with no obvious interesting lateral variations in the interval. Note that when a horizon is picked on a peak of a zero-component section, it corresponds perfectly to a zero crossing on a −90° component section and varies from a peak to a zero crossing on the real seismic data. This suggests that the true formation top is changing its position on the seismic waveform as rock properties are varying laterally. Simple picking of a peak, zero crossing, or trough on conventional seismic data can thus easily be one-fourth of a period off from the correct horizon position, corresponding to as much as half

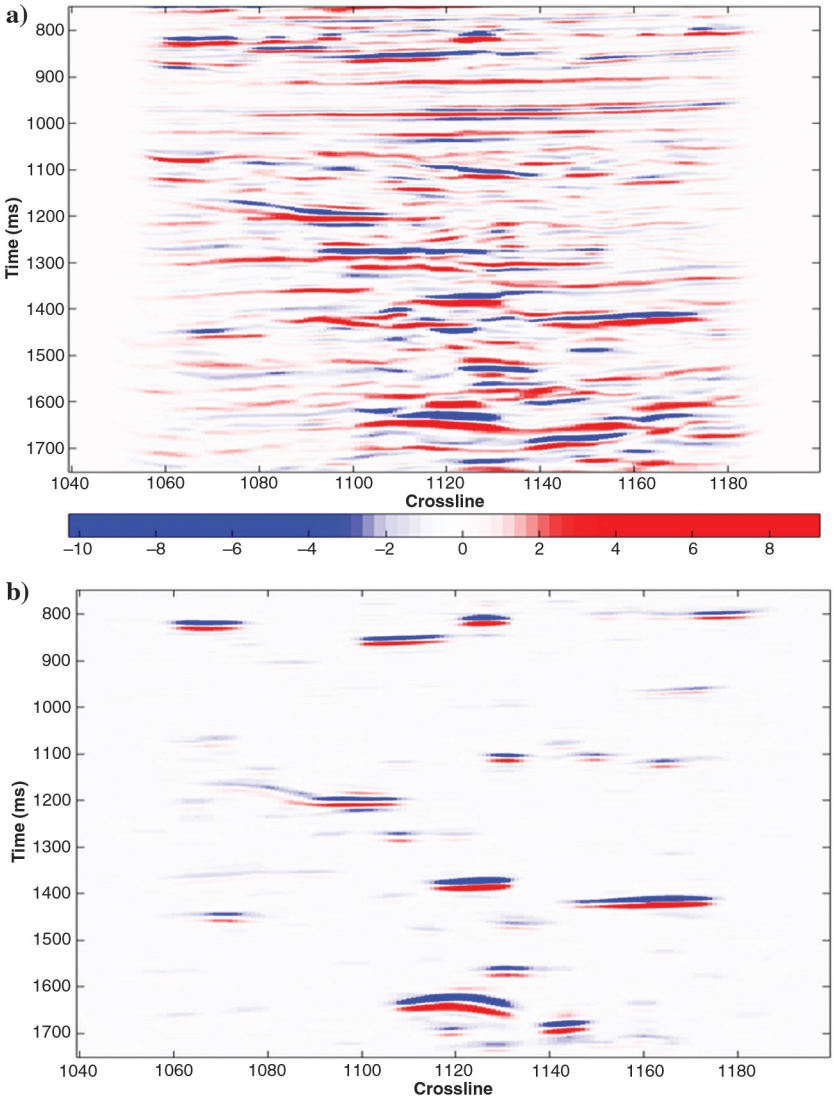

Figure 7. (a) Stacked seismic section and (b) −90° component.

the time thickness of a layer at tuning and more for thinner layers. Such picking errors can wreak havoc in quantitative seismic analysis as well as in mapping of subtle structures. Notice also that although the changes in seismic response are not remarkable as one follows the horizon labeled A across the original seismic section, the −90° component exhibits a very large amplitude change, and in fact it changes sign along the horizon, suggesting

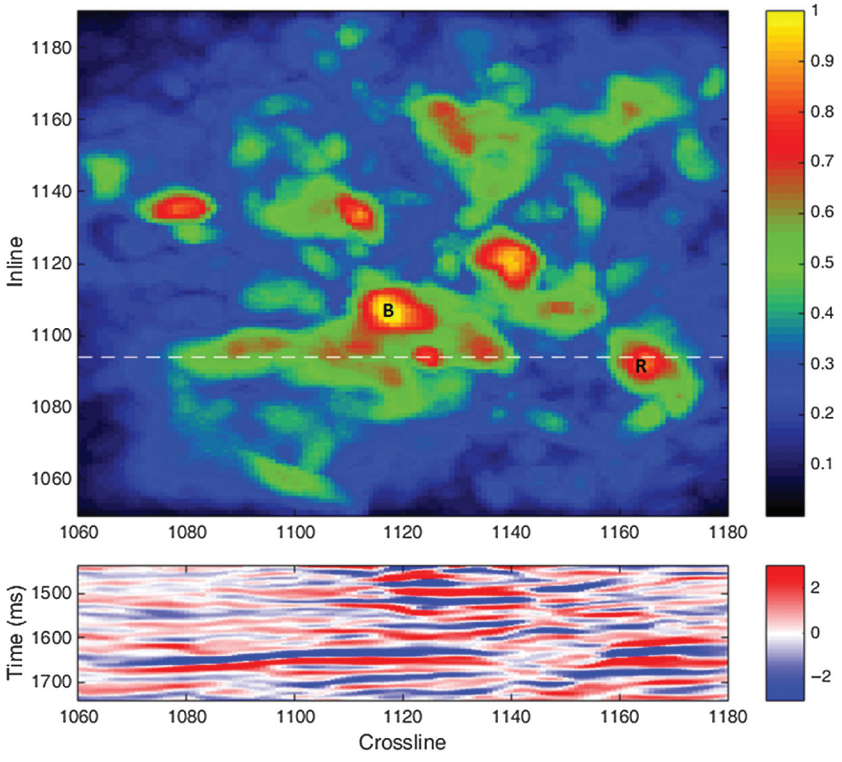

Figure 8. (a) Maximum magnitude map and (b) seismic section extracted from original seismic data along the dashed line. The window for selection of maximum magnitude corresponds to the extent of the seismic data shown. A productive interval is marked with an "R." A bright amplitude is marked with a "B."

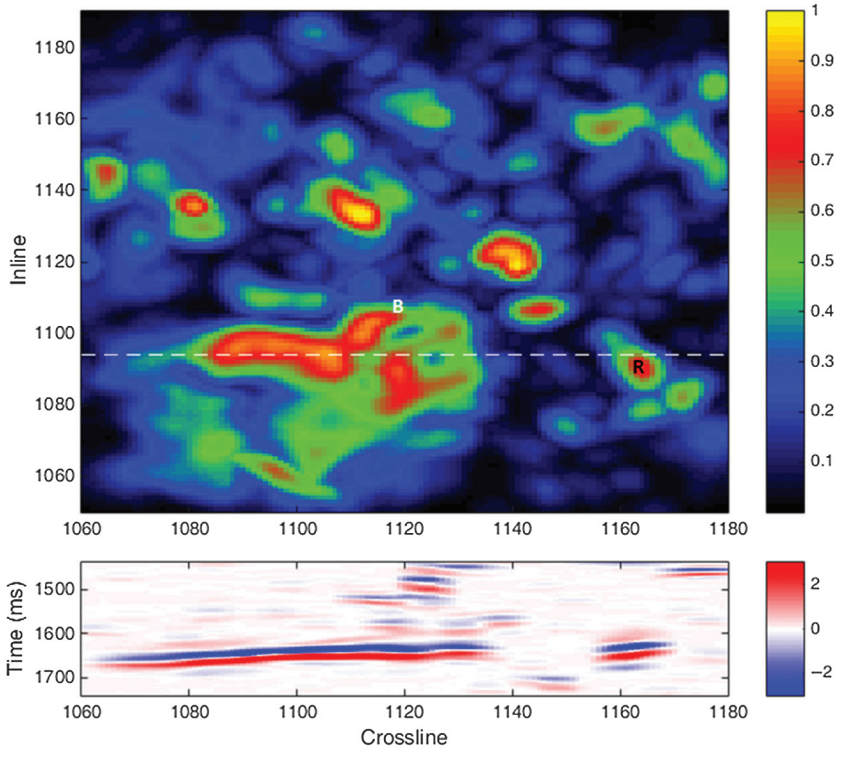

Figure 9. (a) Maximum magnitude map and (b) seismic section extracted from the −90° phase component of the seismic data. The window for selection of maximum magnitude corresponds to the extent of the seismic data shown. The reservoir "R" shows anomalous amplitude on this component. The bright event "B" does not.

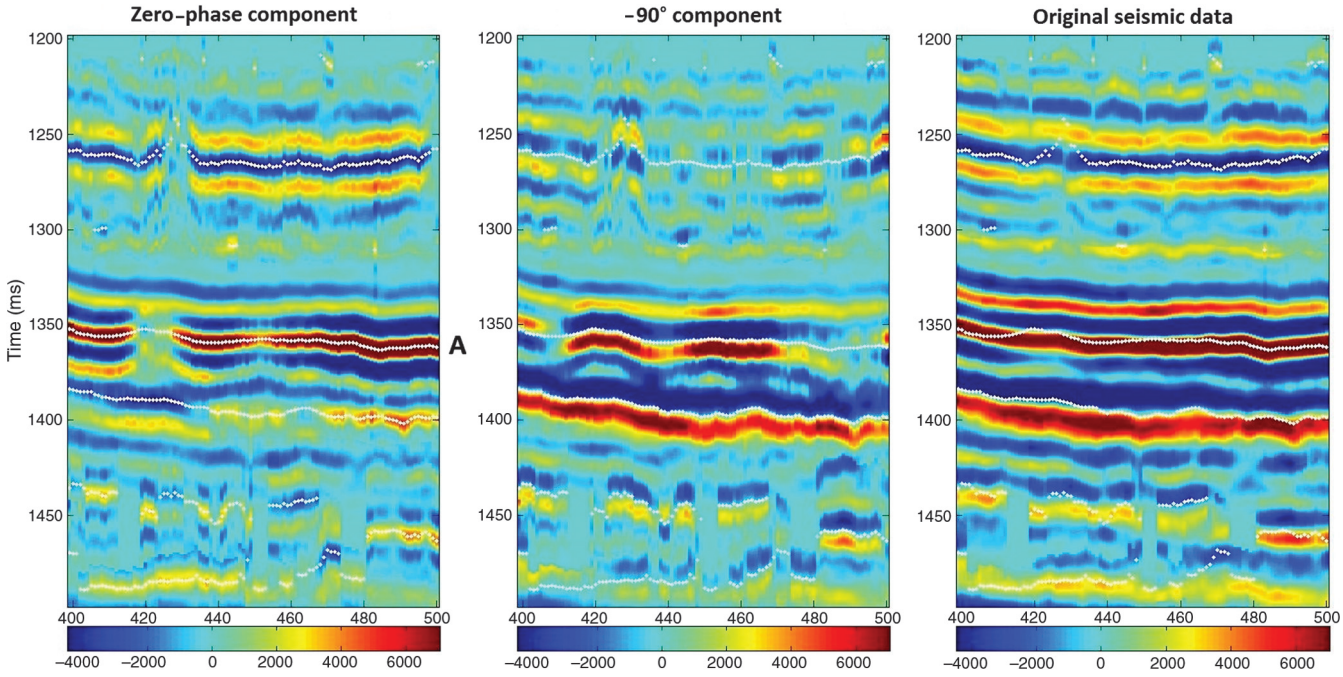

Figure 10. Comparison of zero-phase and summed ±90° phase components to original seismic section. The yellow horizon labeled "A" corresponds to a peak on the zero-phase component, a zero crossing on the 90° section and wanders around on the original seismic data. Along this horizon, a change in sign of the −90° reflection suggests an impedance change from high impedance at the edges to low impedance in the center.

an impedance change within a thin layer from high impedance at the edges to low impedance in the center.

Conclusions

Any seismic trace can be decomposed into a 2D function of amplitude versus time and phase. For seismically thin layers, lateral impedance variations that exhibit negligible amplitude change on a seismic section may exhibit strong amplitude anomalies on specific phase components corresponding to the change in shape of reflection coefficient pairs.

Specific phase components may be diagnostic of particular geologic situations. For example, the phase component corresponding to the phase of the seismic wavelet could indicate isolated interfaces or any other time-symmetrical variation of reflection coefficients. Thus, assuming a zero-phase wavelet, flat spots and unresolved water contacts may show directly on the zero-phase component. Similarly, thin beds and impedance ramps can show up on components that are 90° out of phase with the wavelet. For a zero-phase wavelet, these will be found on the −90 and +90° phase components. Interpretation of layer thickness is thus simplified using phase decomposition.

In the case of bright spots caused by hydrocarbons in thin reservoirs, because these occur when the reservoir is anomalously low impedance, it is safe to assume that the brightening caused by hydrocarbons occurs on the component −90° out of phase with the wavelet. Amplitudes of other phase components associated with bright reflection events, resulting perhaps from differing impedances above and below the reservoir, thus obscure the hydrocarbon signal. Assuming a zero-phase wavelet, bright-spot interpretation is thus greatly simplified on the −90° phase component for thin beds. Amplitude maps for the Teal South Field shows that the lateral distribution of amplitudes is greatly different for the original seismic data and the −90° phase component, exhibiting very different prospectivity and apparent areal distribution of reservoirs.

As impedance changes laterally, the interference pattern for composite seismic events also changes. Thus, waveform peaks, troughs, and zero crossings may not be reliable indicators of formation top locations. As the waveform phase changes laterally, the position of the top on the waveform also changes. By picking horizons on distinct phase components, this ambiguity is removed and more consistent horizon picking is enabled.

References

Chakraborty, A., and D. Okaya, 1995, Frequency-time decomposition of seismic data using wavelet-based methods: Geophysics, **60**, 1906–1916, doi: 10.1190/1.1443922.

Partyka, G., J. Gridley, and J. Lopez, 1999, Interpretational applications of spectral decomposition in reservoir characterization: The Leading Edge, **18**, 353–360, doi: 10.1190/1.1438295.

Pennington, W. D., H. Acevedo, J.J. Haataia, and A. Minaeva, 2001, Seismic time-lapse surprise at Teal South: That little neighbor reservoir is leaking: The Leading Edge, **20**, 1172–1175, doi: 10.1190/1.1487249.

Puryear, C. I., O.N. Portniaguine, C. Cobos, and J.P. Castagna, 2012, Constrained least-squares spectral analysis: Application to seismic data: Geophysics, **77**, no. 5, V143–V167, doi: 10.1190/geo2011-0210.1.

Widess, M., 1973, How thin is a thin bed?: Geophysics, **38**, 1176–1180, doi: 10.1190/1.1440403.

Biographies and photographs of the authors are not available.